LAWRENCE
LIVERMORE
NATIONAL
LABORATORY

LLNL-JRNL-407229

Nanoporous Au: an unsupported pure gold catalyst?

A. Wittstock, B. Neumann, A. Schaefer, K. Dumbuya , C. Kuebel, M.M. Biener, V. Zielasek, H.-P. Steinrueck, M. Gottfried , J. Biener, A. Hamza, M. Bäumer

September 25, 2008

Journal of Physical Chemistry C

Disclaimer

Nanoporous Au: an unsupported pure gold catalyst?

Arne Wittstock[1,2], Björn Neumann[1], Andreas Schaefer[1], Karifala Dumbuya[3], Christian Kübel[4], Monika M. Biener[2], Volkmar Zielasek[1], Hans-Peter Steinrück[3], Michael Gottfried[3], Jürgen Biener[2], Alex Hamza[2], and Marcus Bäumer[1]

[1]*Institute for Applied and Physical Chemistry, University of Bremen, Leobener Strasse NW2, 28359 Bremen, Germany*

[2]*Nanoscale Synthesis and Characterization Laboratory, Lawrence Livermore National Laboratory, P.O. Box 808, Livermore, California 94550, United States of America*

[3]*Universität Erlangen-Nürnberg, Lehrstuhl für Physikalische Chemie II, Egerlandstr. 3, 91058 Erlangen, Germany,*

[4]*Fraunhofer Institute for Manufacturing Technology and Applied Materials Science (IFAM), Adhesive Bonding and Surfaces Division, Wiener Straße 12, 28359 Bremen, Germany*

Abstract

The unique properties of gold especially in low temperature CO oxidation have been ascribed to a combination of various effects. In particular, particle sizes below a few nm and specific particle-support interactions have been shown to play important roles. On the contrary, recent reports revealed that monolithic nanoporous gold (npAu) prepared by leaching a less noble metal, such as Ag, out of the corresponding alloy can also exhibit remarkably high catalytic activity for CO oxidation, even though no support is present. Therefore, it was claimed to be a pure and unsupported gold catalyst. We investigated npAu with respect to its morphology, surface composition and catalytic properties. In particular, we studied the reaction kinetics for low temperature CO oxidation in detail taking mass transport limitation due to the porous structure of the material into account. Our results reveal that Ag, even if removed almost completely from the bulk, segregates to the surface resulting in surface concentrations of up to 10 at%. Our data suggest that this Ag plays a significant role in activation of molecular oxygen. Therefore, npAu should be considered as a bimetallic catalyst rather than a pure Au catalyst.

Keywords

Gold catalysis, CO oxidation, nanoporous gold, dealloying, bimetallic catalysts

Introduction

In recent years, catalysis by gold became an intensively studied topic in research due to its promising applications e.g. in low temperature CO oxidation[1-4], selective oxidation of methanol[5,6], epoxidation of propene[7,8], and water-gas shift reaction[9,10]. Generally, it is believed that catalytic activity of this noble metal only occurs when it is in the form of nm-sized particles supported on a suitable metal oxide support. Numerous studies revealed complex dependencies of the catalytic properties on the size of the particles, the nature of the support and other factors, such as the presence of water in the feed, for instance.[11] The use of some supports, including α-Fe_2O_3 and TiO_2 as well as CeO_2, results in highly active catalysts, whereas catalysts prepared on others, such as Al_2O_3 and SiO_2, showed usually low or no activity.[12] Unfortunately, no consistent picture has arisen so far from the partly deviating results so that the debate regarding the underlying mechanisms still continues.

Consequently, some effort was made to prepare and investigate Au catalysts without any support to assess the activity of pure Au without support effects. Dumesic and coworkers e.g. showed that Au nanotubes embedded in a polycarbonate matrix are active for the oxidation of CO at room temperature.[13] Haruta et al. demonstrated that Au powder consisting of particles in the range of 100 nm prepared by evaporating Au into an inert gas exhibits remarkable catalytic activity.[14] Interestingly, a careful characterization of the material revealed a strong influence of Ag impurities resulting from the manufacturing process.

Another route to unsupported nanostructured Au catalysts only recently proposed in the literature is the preparation of a monolithic nanoporous Au material (npAu) by selectively leaching a less noble metal, such as Ag or Cu, from the corresponding gold alloy.[15] The resulting material exhibits a characteristic spongelike open-cell morphology with a uniform feature size on the nanometer length scale. Depending on the particular preparation conditions, the ligament size can be tailored between 10 nm and 1 micron without changing the relative morphology.[16] As shown by several groups, such a material can exhibit surprisingly high activity for low temperature CO oxidation.[17-21]

Based on these results, several authors claimed that this activity reflects the unique properties of Au in the absence of a support.[19,20] In particular, it was speculated that this system might help to unravel some of the open questions in Au catalysis. If that was true, however, aspects, such as particle size and the role of the support, would have been misinterpreted so far as being essential prerequisites in Au catalysis. Rather, they would be special features of supported systems.

Putting these new materials in the context of previous research, Haruta pointed out that impurities, such as Ag, left over from the preparation may be important ingredients to understand the unique properties of npAu.[22] In particular, if these components are oxidized under reaction conditions or supply activated oxygen, they could play an analogous role as the supports in the case of supported systems.

In some of the previous reports on the catalytic activity of npAu, however, residues of the second metal were not taken into consideration when explaining the catalytic properties[19,20], although a participation in the catalytic cycle is very likely. While CO adsorbs on Au especially on low coordinated sites[23,24] no adsorption of oxygen was found

on single crystal surfaces.[25,26] Only in case of small particles, dissociation becomes feasible.[27] In view of these results, dissociation of O_2 on pure npAu seems rather unlikely to occur. On the other hand, several investigations of Au-Ag bimetallic particle systems on inert supports showed that catalytic activity for CO oxidation can even be obtained if rather large particles (> 30 nm) are used. Moreover, a clear correlation between composition and conversion was detected suggesting the possibility to tune the catalytic properties by changing the Au/Ag ratio.[22,28-32]

Motivated by these results, we aimed at elucidating whether the catalytic behaviour of npAu provides indications for an analogous role of residual Ag left over from the dealloying process for the adsorption and activation of reactants. Using CO oxidation as a probe reaction, we studied the activation of the samples, the reaction kinetics of their steady-state activity and the chemical state under reaction conditions. Moreover, we aimed at studying the ability of the material to adsorb and bind oxygen after exposing it to molecular oxygen and, for comparison, to ozone which is known to be able to deliver atomic oxygen to Au surfaces.[33]

The results of our experiments indicate that npAu is not a pure Au catalyst and imply that Ag is a necessary factor for carrying out oxidation reactions with this material. The remarkable and unexpected high capability of activating molecular oxygen can be easily understood in terms of a bimetallic alloy catalyst in a similar way as was previously reported for bimetallic Au-Ag systems.[22,31,34,35]

Experimental

Disks of npAu with a diameter of 5 mm and a thickness of 200 and 300 microns were prepared by etching Ag-Au alloys in concentrated nitric acid (48 hrs, HNO_3, ~70 wt%, OmniTrace EMD Chemicals). This procedure is very efficient and removes Ag almost quantitatively to concentrations below 1 at% as determined by EDX (energy dispersive x-ray spectroscopy) or AAS (atomic absorption spectroscopy). Samples with a slightly higher residual silver content were obtained by adding $AgNO_3$ to the nitric acid (0.2 M Ag^+). In this way, the silver concentration could be adjusted to concentrations up to 4 at%, as determined by EDX.

The master alloy for all samples was prepared by melting Au and Ag pellets in the desired composition (Ag 70 at%, Au 30 at%). After verification of the alloy composition by EDX the ingots were annealed under an Argon atmosphere for 140 hours at 875 °C. After this homogenization the ingots were rolled, cut into the desired shape and again repeatedly annealed in air for 4 hours at 800 °C.

For structural characterization, the npAu was infiltrated with an epoxy resin (Spoerr) and tempered at 70° C for 8h. Afterwards, ultrathin slices with a nominal thickness of 100-200 nm were prepared by ultramicrotomy at room temperature and transferred on carbon coated copper grids. TEM analysis of the infiltrated npAu was performed using a Tecnai G2 F20 STwin instrument equipped with a Schottky Field Emitter (FEG) and operated at 200 kV. Imaging was performed either in BF-TEM mode or in HAADF-STEM mode with a nominal spot size of 0.5 nm. Analytical work was performed using an EDX detector with a S-UTW window either working in HAADF-STEM mode with a

nominal spot size of 1-2 nm or in BF-TEM mode to look at compositional averages over larger areas.

X-ray photoelectron spectra (XPS) of selected samples were recorded under ultra high vacuum (UHV) conditions (base pressure of the UHV chamber: 10^{-11} mbar) employing a Mg K_α X-ray source at 1253.6 eV and a hemispherical analyzer (Leybold, EA 10 plus). If not stated otherwise, the pass energy was set to 25 eV.

The in-situ XPS measurements were performed with a high-pressure X-ray photoelectron spectrometer, which can be operated in the presence of a reactive gas phase at pressures of up to 1 mbar at the sample; this allows for measurements within the "pressure gap" regime. The apparatus has been described in detail elsewhere.[36] Briefly, the experimental setup is based on a modified hemispherical electron energy analyzer (Omicron EA 125), a modified twin anode X-ray source (Specs) (here used: Al Kα radiation, hν = 1486.6 eV), and several differential-pumping stages between the sample region and the electron detector. The vacuum system has a base pressure in the 10^{-10} mbar range. The reaction gas is provided in-situ by either background dosing or beam dosing; the latter uses a directed gas beam from a tube with a small cross section and permits higher local pressures. In this work, only background dosing was employed. For the general calibration of the energy scale of the spectrometer we used the Fermi edge and the Au $4f_{7/2}$ signal ($E_B \equiv 84.0$ eV) of a clean Au(111) sample.

The catalytic experiments were conducted in a continuous flow reactor especially designed for catalytic experiments with the npAu disks. A scheme of the reactor is shown as inset in *Figure 2 (B)*. The reactor was completely made of glass, and its inner diameter was around 20 mm with a total volume of 26 ml. The inlet tubing and the reactor were

embedded in a liquid bath for precise temperature control. The samples were placed at the lower end of the reactor on a Au plate with an opening in the center. The inlet gas was directed through this opening directly towards the sample, thus avoiding that large parts of the feed bypassed the sample.

If not stated otherwise, the feed consisted of a mixture of CO (4.7 *Linde AG*), N_2 (*Linde AG*, 4.6), and O_2 (*Linde AG*, 4.5). The total flow was always set to 50 sccm. The composition was precisely controlled via mass flow controllers (Maettig Bronkhorst, Netherlands). For experiments using ozone as a supply for atomic oxygen, we used the same apparatus in connection with an ozone generator (Type 802 N, BMT Messtechnik Berlin) and an ozone analyzer (Type 964, BMT Messtechnik Berlin).

Results

Structural characterization

The morphology of nanoporous Au obtained by dealloying Ag70Au30 alloy samples in nitric acid is demonstrated by the SEM and TEM micrographs shown in Figure 1. The material exhibits a characteristic three-dimensional bi-continuous nanoporous structure with a porosity of ~70 % and a uniform feature size of 30 – 50 nm that can be very reproducibly prepared.[37] (Different samples are virtually not distinguishable with respect to their morphology.) The residual silver content of material which was dealloyed for 48 h in concentrated HNO_3 is typically 1 at%. To study the effect of residual Ag we also prepared samples with Ag contents up to 4 at% (homogeneously distributed throughout the sample) by adding $AgNO_3$ to the HNO_3 solution.

Reaction kinetics

As reported previously[18], pristine npAu samples have to be activated before they exhibit catalytic activity for CO oxidation at room temperature. The CO_2 signal as recorded at the reactor outlet during activation of a npAu sample with a residual Ag content of 4 at% at 80 °C is shown in Figure 2 (A). The increasing CO_2 signal after two to three hours indicates the onset of activation. The activity continues to increase over the next few hours finally reaching either a plateau or, more often, passing a transient activity maximum after which the CO_2 signal decreases again. When the temperature is decreased at this point (for example to 20 °C) the conversion rate usually increases again and is subsequently stable.

It is interesting to note, however, that not all samples could be activated by this procedure. In particular, samples which were stored for several weeks after being dealloyed, could often not be activated.

For samples that could be activated the kinetics of the reaction was studied in detail. For this purpose, one reaction partner (either CO or O_2) was kept in excess (constant high partial pressure), whereas the other one was systematically increased from very low to very high concentrations. A typical O_2 variation experiment (fixed CO concentration) for a sample with 4 at% Ag is shown in Figure 2 (B). The signal intensity of the product CO_2 follows (delayed by the retention time of the gases in the reactor) the O_2 concentration which was increased in a stepwise manner. Note that the concentration was only changed after observing a steady state for at least five minutes.

For further analysis of the data, the measured CO_2 concentrations at steady state were converted into a conversion rate and referred to the mass of catalyst and the surface area (3.7 m^2/g as measured by BET), respectively.

Figure 3 (A) shows the results for increasing CO concentrations in an O_2 excess at 20 °C. Even though the plot already reveals a linear dependence of the rate on the CO concentration, we re-plotted the data in log-log coordinates to determine the reaction order in more detail (see inset). As long as the O_2 concentration is not limiting the rate (up to ~ 8 mol/m^3 CO), the total reaction order corresponds to the reaction order of CO under these conditions. Evaluating the slope of the straight line (1.04) confirms that the CO reaction order is 1.

Figure 3 (B) shows the results for the analogous O_2 variation experiment (fixed CO concentration). At low concentrations the increase in conversion is larger than for higher

concentrations. The overall shape of the curve suggests a parabolic dependence, i.e. a reaction order of 0.5 which is indeed confirmed by the double logarithmic plot (see inset).

Similar experiments were performed for a number of samples. The results clearly demonstrated that the kinetic parameters *are not constant*, but vary from sample to sample. For the reaction order of CO, in particular, values between 0.5 and 1 were found with a tendency of higher values for the samples with higher silver concentrations. For the reaction order of oxygen, on the other hand, no such large variations were observed. Here, values close to 0.5 were found in all cases.

So far we discussed only experiments where one reaction partner was supplied in large excess. In addition, we performed experiments where one gas concentration was held constant at lower levels while the other concentration was varied. Figure 2 (C) shows results obtained for different constant oxygen concentrations. Notably, at low CO concentrations, the conversion increases linearly and is apparently *independent* from the actual amount of O_2 even though the O_2 concentration spans a range from 2 vol% to over 60 vol%, i.e. is increased by a factor of 30. This behavior suggests that CO and oxygen *do not compete* for adsorption sites on the surface. For higher CO concentrations the conversion reaches a plateau which increases with increasing O_2 concentrations as a result of the limitation of the reaction by the oxygen supply.

While the reaction shows almost no temperature dependence above 20 °C, a measurable dependence below 0 °C allowed us to determine the activation energy of the reaction. For this purpose, the temperature was first lowered to 253 K and than continuously increased to 273 K, while recording the CO_2 formed at the reactor outlet with a feed of 2 vol% CO and oxygen excess (Figure 4 (A)). Assuming an Arrhenius type temperature dependence

of the rate, the slope of the (natural) logarithm of the rate as a function of the inverse temperature provides the (apparent) activation energy E_a(app). For the sample described above, an E_a(app) of ~ 8 kJ/mol was determined in this way (see Figure 4 (B)). Such a low value is also compatible with the finding that the reaction is temperature independent at room temperature. Under these conditions, the exponential factor in the Arrhenius equation is essentially 1. As in the case of the reaction orders, the measured activation energies scattered to some degree from sample to sample with values as low as 4 kJ/mol.

Role of mass transport limitation

In a previous publication, it was already pointed out that mass transport limitation in the nanoporous Au material may affect the measured kinetics (activity, reaction order) and thus needs to be taken into account when drawing conclusions regarding the actual kinetics of the reaction.[17] Usually, the effect of mass transport limitation on the apparent reaction order and activation energy of heterogeneously catalyzed reactions is very difficult to analyze. Here, however, we take advantage of the well-defined structure of npAu to estimate the degree of mass transport limitation by applying a simple diffusion-reaction model based on reasonable assumptions.[38-40] We can treat CO and oxygen independently since no indications for competitive adsorption of the two reactants were found.

We address the degree of mass transport limitation by using the so-called Thiele modulus which is a dimensionless number that describes the ratio of reaction rate to the diffusion rate. Assuming pseudo-first order reaction conditions, that is, one reaction partner is in large excess, the Thiele modulus Φ can be expressed as:

$$\Phi \equiv a \cdot \sqrt{\frac{k \cdot c_g^{m-1}}{D}} \,. \qquad (1)$$

Here, a is the aspect ratio of the pores, and k is the reaction constant (m/s), C_g is the gas phase concentration (mol/m^3), m is the reaction order, and D is the diffusion coefficient. Note that the Thiele modulus is only independent of the gas phase concentration in the case of a first order reaction.[40]

The Thiele modulus expresses the degree of limitation by mass transport, the higher this value the more the reaction rate is dominated by mass transport through the pores. One can say that if the Thiele modulus is between 0.2 and 3 the overall reaction rate is influenced by mass transport phenomena; a Thiele modulus of over 3 means that the consumption of reactants is so fast, that only mass transport i.e. supply of reactants into the pores is rate limiting. The effect of mass transport on the observed kinetic parameters is demonstrated by the examples presented in Table 1. For a reaction order of 1, as determined as an upper bound for CO, the order is not affected by mass transport. As far as the activation energy is concerned, the model predicts that E_{act} is two times larger than the measured (apparent) activation energy if mass transport limits the reaction ($\Phi > 3$).[40] If, however, the reaction order is different from 1, the measured apparent order is different from the "true" reaction order of the surface reaction. In particular, an apparent order of 0.5 corresponds to a true reaction order of 0, that is, the rate is independent from the gas phase concentration.

To assess if, and to what extend, our measured reaction kinetics is influenced by mass transport limitations, we calculated the Thiele modulus for both CO and O_2. Specifically, we use the following assumptions: First, we approximate the porosity of npAu by capillaries with length L and radius r, in which case the aspect ratio a can be expressed as

$2L/\sqrt{r}$. This yields an aspect ratio of 1.6-2.5 $m^{½}$ if we assume 100-150 μm long (half of the sample thickness) and 30 nm wide capillaries. Furthermore, assuming Knudsen diffusion, the coefficient D in a highly porous material such as np-Au can be expressed by[41]

$$D = \varepsilon_p \frac{D_K}{\tau}, \qquad (2)$$

where D_K is the Knudsen diffusion coefficient (m^2/s), ε_p is the porosity of the material (0.7 in our case) and τ is the so called tortuosity factor (set to 5) which accounts for the tortuous path of a molecule through the porous network (actual distance a molecule must travel divided by the film thickness). Finally, the Knudsen diffusion coefficient D_K is calculated by

$$D_K = 3.067 \cdot r \cdot \sqrt{\frac{T}{M}}, \qquad (3)$$

where T is the temperature and M the molecular mass of the gas molecules. For our specific example, the diffusion coefficients D of oxygen and CO at RT are $6.2 \cdot 10^{-7}$ $m^2 \cdot s^{-1}$ and $6.6 \cdot 10^{-7}$ $m^2 \cdot s^{-1}$, respectively.[1]

Based on equations (1) to (3) and taking the data set of *Figure 3* as an example, a Thiele modulus of 6.3 is obtained for CO, that is, the system is indeed mass transport dominated. In this case, the efficiency η (ratio of reaction velocity of un-influenced and

[1] However, one should note that in case of large adsorption energies (pronounced sticking) pure Knudsen diffusion is no longer an appropriate description of mass transport through nanopores. (42) Norberg, P.; Ackelid, U.; Lundstoem, I.; Petersson, L.-G. *J. Appl. Phys.* **1997**, *81*, 2094.. Indeed, measurements of oxygen diffusion through nano-machined straight pores coated with Pt demonstrated that the effective diffusion through nanopores can be ten times slower than predicted by pure Knudsen diffusion. (42) Norberg, P.; Ackelid, U.; Lundstoem, I.; Petersson, L.-G. *J. Appl. Phys.* **1997**, *81*, 2094. In the present case, an influence for CO might be expected, since a large fraction of the surface atoms of npAu should consist of undercoordinated step and kink sites with adsorption energies in the range of 39-51 kJ/mol, corresponding to an average residence time between 10^{-2} and 1 ms. (23) Yim, W. L.; Nowitzki, T.; Necke, M.; Schnars, H.; Nickut, P.; Biener, J.; Biener, M. M.; Zielasek, V.; Al-Shamery, K.; Kluner, T.; Baumer, M. *Journal of Physical Chemistry C* **2007**, *111*, 445. Likewise, for oxygen sites with a strong interaction are probably present on the surface as well.

influenced reaction) of the catalyst is just 0.16, i.e. the (averaged) concentration of reactant gas within the pores is roughly only one fifth of the concentration in the outer gas phase. The calculated cross-sectional concentration profile of CO in 200-μm-thick sample of npAu is shown in Figure 5 and illustrates the depletion of CO in the center of the sample. Note that the effect becomes even more pronounced for ultrafine npAu material prepared by electrochemically dealloying (15 nm pores)[20], where η is further decreased by a factor of four. In the same way, it was confirmed that also for oxygen the Thiele modulus is above 3 in the relevant concentration range of 1 to 5 mol/m^3 (Figure 3 (B)). Thus, for both reactants, mass transport limitation dominates, meaning that for CO the apparent reaction order between 0.5 and 1 correspond to actual orders between 0 and 1 and the actual activation energy is two times larger than the measured ones (i.e. 8 kJ/mol correspond to 16 kJ/mol), whereas the apparent reaction order of 0.5 for O_2 corresponds to an actual reaction order of 0.

Nature of oxygen species on the surface

An important question in Au catalysis concerns the activation of molecular oxygen. While no chemisorption of molecular oxygen on planar Au surfaces is observed[43,44], low coordinated gold species were proposed to account for the adsorption and activation of O_2 on Au nanoparticles.[45] In the case of npAu with ligaments in the range of several 10 nm, however, this explanation is unlikely. Furthermore, it was speculated that Au oxide clusters, once formed under catalytic conditions, are capable of dissociating molecular oxygen so that a constant steady state coverage of oxygen atoms on the surface can be maintained under reaction conditions.[46] In this context, it is interesting to note that Xu et al. discussed a positively charged Au species formed under dealloying conditions.[19] Since

cationic gold was frequently discussed to be an ingredient for catalytic activity, it could play a role also in the case of npAu.

In order to check whether stable Au oxide species can be generated on npAu and whether they can initiate a stable steady state conversion, we treated a sample with ozone, which is known to decompose readily on Au surfaces and to form Au oxide species.[33] In a first step, we exposed the sample to 0.3 vol% of ozone in a feed of synthetic air for 30 minutes. Subsequently, the surface concentration of oxygen was measured by recording the amount of CO_2 formed when reacting the oxide surface species away with CO. (To prevent direct reaction of ozone with CO, the reactor was thoroughly purged with synthetic air for 40 minutes after the ozone treatment.) The resulting CO_2 peak is shown in Figure 6. Based on the total number of Au surface atoms (spec. surface 3.7 m^2/g, $1.4 \cdot 10^{15}$ at/cm^2 (Au(111)), M_{Sample}=29.5 mg) and assuming that every adsorbed oxygen atom reacts with one CO molecule, an oxygen surface coverage of about 1 ML can be calculated, in good agreement with experiments on single crystal surfaces. [33]

Next, we repeated the experiment using molecular oxygen instead of ozone. Under these conditions, a CO_2 peak was *not* detected revealing that molecular oxygen is not able to form a stable atomic oxygen species in a significant amount (~ 0.1 ML) on npAu.

To evaluate the impact of a pre-coverage of the surface with atomic oxygen on activation of molecular oxygen we used an inactive sample, i.e. a sample which showed no conversion of CO at room temperature. After ozone treatment and purging, CO and oxygen were simultaneously added to the gas stream. This resulted in a CO_2 burst similar to Figure 6 but *no continuous* activity with respect to CO oxidation. These observations imply that neither an initially present charged Au species nor atomic oxygen previously

deposited on the surface are able to initiate a continuous oxidation, i.e. activation of molecular oxygen on npAu.

The presence of Ag

As discussed before, npAu prepared by free corrosion contains almost no silver in the bulk. However, residual traces of Ag could still be detected by EDX and AAS. To estimate the amount of Ag present on (or near to) the surfaces of npAu (which is the Ag species of interest in terms of catalysis) we employed X-ray photoelectron spectroscopy (XPS) which is more surface sensitive than EDX.

A quantitative analysis of XP spectra recorded in the Ag 3d and Au 4d/4f regions of catalytically active samples (activity was checked before and after XPS characterization) which had a very low concentration of residual Ag, as judged by EDX, revealed a Ag concentration of 7 at% (using the integrated signal intensity of the Ag 3d and Au 4d peaks and the appropriate sensitivity factors). Since EDX results indicated an overall volume composition below 1 at%, this points to an enrichment of Ag close to the surface. This is consistent with the lower surface energy of Ag which can lead to Ag surface segregation.[47]

In order to identify transient changes in the chemical composition of the surface *during the reaction*, we performed in-situ XPS measurements at varying pressures of up to 1 mbar (see experimental section for details). In the case of the pristine sample, the Ag $3d_{5/2}$ signal is found at 367.6 eV, which suggests an oxidized state of the Ag at first sight.[48] It has to be noted, however, that binding energy shifts in this direction have been reported for bimetallic Au-Ag particles where they have been attributed to re-

hybridization effects in the alloy (reduction of electron density at the silver). In case of the Au 4f signal both shape and BE point toward metallic Au.[49]

The presence of O_2, CO, or a mixture of both has only little effect on the Au4d and Au4f signals (data not shown), while significant changes are observed in the Ag3d region (*Figure 7*). First, we performed ex-situ XPS measurements following exposure to CO and O_2: The spectra A, B, and C in Figure 7 show the Ag3d signal in vacuo, after exposure to 1 mbar CO for one hour, and exposure to 1 mbar O_2 for the same period of time, respectively. The differences between these three XP spectra are obviously very small, indicating that *no permanent* changes are induced by the presence of the reactive gases. However, the spectra D and E, taken in the presence of 1 mbar O_2 and 1 mbar of a 1:1 mixture of O_2 and CO, respectively, show significant *transient* changes in the Ag3d signal. Most obvious is the broad shoulder in the range of lower binding energies (363 – 366 eV), which cannot be attributed to chemisorbed oxygen on Ag nor to Ag_2O or AgO species. These species show smaller Ag3d binding energy shifts as compared to Ag^0 (less than 1 eV towards lower binding energy[50], whereas the shoulder in spectra D and E is shifted by 1.5 – 4.5 eV relative to the Ag3d main peak. Apparently, a specific Ag surfaces species (or several different surface species) is formed in the presence of O_2 or O_2/CO. At the present stage, we can only speculate on its chemical nature. A possible explanation for the large shift towards lower binding energy is a final state effect resulting from an Ag-adsorbate complex which is less efficiently screened than the majority of the Ag atoms embedded in the Au matrix. The appearance of the shoulder is fully reversible (spectrum F, taken after the in-situ XPS measurements), indicating that the observed effects are not induced by X-rays or secondary electrons.

Note that during and after the in-situ XPS measurements (curves D-F in *Figure 7*, left) a shift of the main Ag $3d_{5/2}$ signal towards lower binding energy by ca. 0.5 eV occurs. Besides slow oxidation of the Ag in the sub-surface region and beam induced effects, the possible reasons for this shift may also include gas-phase induced changes of the surface composition.

Discussion

The high catalytic activity of nanoporous Au as evidenced by the results of the present work and previous reports in the literature is surprising at first sight. Many criteria which are usually considered to be mandatory for Au catalysis are not fulfilled by this material. Neither is the size of the ligaments in the range of few nanometers nor is an oxidic support necessary to obtain extremely high conversion rates. In an attempt to assess the overall catalytic activity of the material, we calculated the turn-over-frequencies (TOF), i.e. the number of product molecules (CO_2) formed per surface atom per second. For the maximal conversion of $12 \cdot 10^{-6}$ mol/(s·m^2) in oxygen excess (see Figure 3 (A)) we obtain a TOF of 0.5 s^{-1} ($1.4 \cdot 10^{15}$ at/cm^2; Au(111)). Considering that the observed rate is limited by mass transport ($\eta = 0.16$) the actual TOF is ~ 3 s^{-1}. This number is in good accordance to reported numbers for Au particles on a TiO_2 support.[51] As, however, it cannot be expected that every surface Au atom is taking part in the catalytic cycle, the real TOF per active surface site will be significantly higher.

Of course, it is an obvious question whether the catalytic activity of npAu is based on the presence of Ag at the surface. It was Haruta who raised questions with respect to the statement of various reports in the literature that npAu is a “supportless” Au catalyst allowing studying the catalytic activity of “pure” Au. In this context, it is important to

note that, according to the in-situ XPS characterization, Ag is present at the surface in significant amounts and that its chemical state is transiently influenced by the presence of the reactive gas phase.

Several investigations carried out for particle systems showed that the catalytic activity of Au with respect to CO oxidation is significantly enhanced by alloying Au with Ag.[22,28-32] In this case, even comparably large particles in the range of a few 10 nm were found to be highly active, whereas pure Au particles in that size regime are known to be inactive.[52] Wang and coworker ascribed the superior catalytic properties to the unique capability of the bimetallic system to adsorb and activate oxygen.[29] On the basis of DFT calculations they could show that O_2 is distinctly stronger adsorbed on the Au-Ag alloy than on either of the pure metals. In addition, co-adsorption of CO and O_2 on adjacent Au and Ag sites – oxygen on Ag and CO on Au - turned out to be more preferred on the bimetallic system than on pure Au and Ag. Thus, according to the work of these authors, the presence of Ag on the surface of npAu should have a strong impact on the catalytic performance: strong co-adsorption and concomitant activation of oxygen by transfer of electron density into the anti-bonding π^* state of the oxygen molecule should cause high reactivity with respect to oxygen-atom transfer. [29,30]

A number of observations substantiate the assumption that the catalytic activity of npAu is indeed caused by the simultaneous presence of Ag. In our investigation all samples had to be activated before catalytic activity was detected. Some samples showed even no activity at all when they were previously exposed to ambient air for a long period of time. Structural characterization of active and inactive samples revealed no distinct differences in the morphology of the samples. Since the morphology determines the

number of undercoordinated Au sites, this finding implies that catalytic activity is not a unique feature of the special surface geometry of the material. Most likely it is dependent on the distribution of Ag and its chemical state. Note that the experiments with ozone as a supply of atomic oxygen showed that neither adsorbed hydrocarbons, which can be immediately reacted away with the atomic oxygen forming CO_2, nor an oxidized state of gold are likely explanations for catalytic (in)activity.

Moreover, the observed reaction kinetics for O_2 and CO are not compatible with most of the data reported for supported Au particles.[52] In particular, there is the exceptional reaction order for oxygen, which is zero, if mass transport limitation is properly taken into account. A reaction order of zero implies that adsorption sites are rapidly saturated, meaning that only a minority of the surface sites is able to actively chemisorb molecular oxygen. This is in line with the fact that Ag is significantly less abundant on the surface than Au. The mechanism as proposed by Wang et al. for bimetallic AuAg particles, which assumes oxygen activation on Ag and CO adsorption on Au is also compatible with the observation that CO and O_2 do not compete for adsorption sites.

Furthermore, the variation of the reaction order of CO for different samples does not fit to the picture of a pure gold catalyst, where CO and oxygen adsorb adjacently on Au and react by a Langmuir-Hinshelwood mechanism.[53] Changing reaction orders have for example been reported for CO oxidation on Pt where oxygen forms islands with which mobile CO molecules can react at the perimeter.[54,55] In a similar way, it can be expected that the distribution of Ag (forming larger or smaller islands with different perimeters) supplying the oxygen affects the kinetics and thus the order.

Finally, the in-situ XPS measurements reveal that the chemical state of parts of the Ag at the surface undergoes major changes, when the material is exposed to a mixture of O_2 and CO at pressures of up to 1 mbar. This is in agreement with titration experiments showing that no stable oxygen species is involved in the reaction. The exact role of the transient Ag species detected by HP-XPS in the reaction is subject to further investigation.

In summary, the catalytic behavior of the material in combination with the spectroscopic data and the relevant literature leads to the conclusion that npAu is not a pure, un-supported Au catalyst. Rather, it has to be considered as a bimetallic catalytic system. Further studies are under way to clarify the correlation between the catalytic properties of npAu and the specific bimetallic composition in more detail.

Conclusion

We studied the morphology, surface composition and catalytic properties of nanoporous gold (npAu), which was produced by chemical de-alloying of a AuAg alloy. In particular, we focused on the reaction kinetics, the role of mass transport limitation, and transient changes in the Ag core levels under reaction conditions, using in-situ XPS. The results strongly suggest that the catalytic activity of npAu is related to the presence of residual Ag, which is enriched at the surface of the nanopores by a factor of up to 10 compared to the bulk concentration.

Acknowledgements

Work at LLNL was performed under the auspices of the U.S. DOE by LLNL under Contract DE-AC52-07NA27344.

References

(1) Haruta, M.; Kobayashi, T.; Sano, H.; Yamada, N. *Chemistry Letters* **1987**, 405.

(2) Ishida, T.; Haruta, M. *Angewandte Chemie-International Edition* **2007**, *46*, 7154.

(3) Campbell, C. T. *Science* **2004**, *306*, 234.

(4) Chen, M. S.; Goodman, D. W. *Science* **2004**, *306*, 252.

(5) Abad, A.; Concepcion, P.; Corma, A.; Garcia, H. *Angewandte Chemie-International Edition* **2005**, *44*, 4066.

(6) Chang, F. W.; Yu, H. Y.; Roselin, L. S.; Yang, H. C.; Ou, T. C. *Applied Catalysis a-General* **2006**, *302*, 157.

(7) Sinha, A. K.; Seelan, S.; Tsubota, S.; Haruta, M. *Topics in Catalysis* **2004**, *29*, 95.

(8) Sinha, A. K.; Seelan, S.; Tsubota, S.; Haruta, M. *Angewandte Chemie-International Edition* **2004**, *43*, 1546.

(9) Fu, Q.; Saltsburg, H.; Flytzani-Stephanopoulos, M. *Science* **2003**, *301*, 935.

(10) Rodriguez, J. A.; Liu, R.; Hrbek, J.; Perez, M.; Evans, J. *Journal of Molecular Catalysis a-Chemical* **2008**, *281*, 59.

(11) Liu, L. M.; McAllister, B.; Ye, H. Q.; Hu, P. *Journal of the American Chemical Society* **2006**, *128*, 4017.

(12) Weiher, N.; Bus, E.; Delannoy, L.; Louis, C.; Ramaker, D. E.; Miller, J. T.; van Bokhoven, J. A. *Journal of Catalysis* **2006**, *240*, 100.

(13) Sanchez-Castillo, M. A.; Couto, C.; Kim, W. B.; Dumesic, J. A. *Angewandte Chemie-International Edition* **2004**, *43*, 1140.

(14) Iizuka, Y.; Kawamoto, A.; Akita, K.; Date, M.; Tsubota, S.; Okumura, M.; Haruta, M. *Catalysis Letters* **2004**, *97*, 203.

(15) Erlebacher, J.; Aziz, M. J.; Karma, A.; Dimitrov, N.; Sieradzki, K. *Nature* **2001**, *410*, 450.

(16) Biener, J.; Hodge, A. M.; Hayes, J. R.; Volkert, C. A.; Zepeda-Ruiz, L. A.; Hamza, A. V.; Abraham, F. F. *Nano Letters* **2006**, *6*, 2379.

(17) Jurgens, B.; Kubel, C.; Schulz, C.; Nowitzki, T.; Zielasek, V.; Biener, J.; Biener, M. M.; Hamza, A. V.; Baumer, M. *Gold Bulletin* **2007**, *40*, 142.

(18) Zielasek, V.; Jurgens, B.; Schulz, C.; Biener, J.; Biener, M. M.; Hamza, A. V.; Baumer, M. *Angewandte Chemie-International Edition* **2006**, *45*, 8241.

(19) Xu, C.; Xu, X.; Su, J.; Ding, Y. *Journal of Catalysis* **2007**, *252*, 243.

(20) Xu, C. X.; Su, J. X.; Xu, X. H.; Liu, P. P.; Zhao, H. J.; Tian, F.; Ding, Y. *Journal of the American Chemical Society* **2007**, *129*, 42.

(21) Kameoka, S.; Tsai, A. P. *Catalysis Letters* **2008**, *121*, 337.

(22) Haruta, M. *Chemphyschem* **2007**, *8*, 1911.

(23) Yim, W. L.; Nowitzki, T.; Necke, M.; Schnars, H.; Nickut, P.; Biener, J.; Biener, M. M.; Zielasek, V.; Al-Shamery, K.; Kluner, T.; Baumer, M. *Journal of Physical Chemistry C* **2007**, *111*, 445.

(24) Gottfried, J. M.; Schmidt, K. J.; Schroeder, S. L. M.; Christmann, K. *Surface Science* **2003**, *536*, 206.

(25) Meyer, R.; Lemire, C.; Shaikhutdinov, S. K.; Freund, H. *Gold Bulletin* **2004**, *37*, 72.

(26) Gottfried, J. M.; Schmidt, K. J.; Schroeder, S. L. M.; Christmann, K. *Surface Science* **2003**, *525*, 184.

(27) Fernandez, E. M.; Ordejon, P.; Balbas, L. C. *Chemical Physics Letters* **2005**, *408*, 252.

(28) Liu, J. H.; Wang, A. Q.; Chi, Y. S.; Lin, H. P.; Mou, C. Y. *Journal of Physical Chemistry B* **2005**, *109*, 40.

(29) Wang, A. Q.; Chang, C. M.; Mou, C. Y. *Journal of Physical Chemistry B* **2005**, *109*, 18860.

(30) Wang, A. Q.; Hsieh, Y.; Chen, Y. F.; Mou, C. Y. *Journal of Catalysis* **2006**, *237*, 197.

(31) Wang, A. Q.; Liu, J. H.; Lin, S. D.; Lin, T. S.; Mou, C. Y. *Journal of Catalysis* **2005**, *233*, 186.

(32) Lim, D. C.; Lopez-Salido, I.; Dietsche, R.; Kim, Y. D. *Surface Science* **2007**, *601*, 5635.

(33) Saliba, N.; Parker, D. H.; Koel, B. E. *Surface Science* **1998**, *410*, 270.

(34) Nakatsuji, H.; Hu, Z. M.; Nakai, H.; Ikeda, K. *Surface Science* **1997**, *387*, 328.

(35) Kondarides, D. I.; Verykios, X. E. *Journal of Catalysis* **1996**, *158*, 363.

(36) Pantforder, J.; Pollmann, S.; Zhu, J. F.; Borgmann, D.; Denecke, R.; Steinruck, H. P. *Review of Scientific Instruments* **2005**, *76*, 9.

(37) Hodge, A. M.; Hayes, J. R.; Caro, J. A.; Biener, J.; Hamza, A. V. *Advanced Engineering Materials* **2006**, *8*, 853.

(38) Petersen, E. E. *Chemical Engineering Science* **1965**, *20*, 587.

(39) Thiele, E. W. *Industrial and Engineering Chemistry* **1939**, *31*, 916.

(40) John Meurig Thomas, W. J. T. *Principle and Practice of Heterogeneous Catalysis*Weinheim, New York, Basel, Cambridge, Tokyo, October 1996.

(41) Mizushima, Y.; Hori, M. *Journal of Materials Science* **1995**, *30*, 1551.

(42) Norberg, P.; Ackelid, U.; Lundstoem, I.; Petersson, L.-G. *J. Appl. Phys.* **1997**, *81*, 2094.

(43) Sault, A. G.; Madix, R. J.; Campbell, C. T. *Surface Science* **1986**, *169*, 347.

(44) Gottfried, J. M.; Schmidt, K. J.; Schroeder, S. L. M.; Christmann, K. *Surface Science* **2002**, *511*, 65.

(45) Janssens, T. V. W.; Clausen, B. S.; Hvolbaek, B.; Falsig, H.; Christensen, C. H.; Bligaard, T.; Norskov, J. K. *Topics in Catalysis* **2007**, *44*, 15.

(46) Quek, S. Y.; Friend, C. M.; Kaxiras, E. *Surface Science* **2006**, *600*, 3388.

(47) Skriver, H. L.; Rosengaard, N. M. *Physical Review B* **1992**, *46*, 7157.

(48) Weaver, J. F.; Hoflund, G. B. *Chemistry of Materials* **1994**, *6*, 1693.

(49) Lim, D. C.; Lopez-Salido, I.; Dietsche, R.; Bubek, M.; Kim, Y. D. *Surface Science* **2006**, *600*, 507.

(50) Hoflund, G. B.; Hazos, Z. F.; Salaita, G. N. *Physical Review B* **2000**, *62*, 11126.

(51) Berlowitz, P. J.; Peden, C. H. F.; Goodman, D. W. *Journal of Physical Chemistry* **1988**, *92*, 5213.

(52) Bond, G. C.; Thompson, D. T. *Catalysis Reviews-Science and Engineering* **1999**, *41*, 319.

(53) Dekkers, M. A. P.; Lippits, M. J.; Nieuwenhuys, B. E. *Catalysis Today* **1999**, *54*, 381.

(54) Wintterlin, J.; Volkening, S.; Janssens, T. V. W.; Zambelli, T.; Ertl, G. *Science* **1997**, *278*, 1931.

(55) Gland, J. L.; Kollin, E. B. *Journal of Chemical Physics* **1983**, *78*, 963.

Tables

Table 1: Dependency of kinetic parameters on mass transport limitation.[40]

	Not limited ($\Phi \sim 0.2$)	Limited ($\Phi > 3$)
Reaction Order 0	Remains Order 0	Appears as Order 0.5
Reaction Order 1	Remains Order 1	Remains Order 1
Activation Energy	Apparent number	Double of the apparent number

Figure Captions

Figure 1: Morphological characterization of npAu by SEM (upper section) and TEM/EDX (lower section).

Figure 2: Catalysis: (A) Typical run of the CO_2 signal during activation of a npAu disk. (B) Run of CO_2 signal (outlet) and corresponding O_2 set value (inlet) (CO as carrier gas, reactor temperature 20 °C). (C) Concentration of CO_2 as a function of the CO at the inlet for different fixed O_2 concentrations (reactor temperature 20 °C).

Figure 3: The conversion referred to the mass of catalyst (A) as a function of CO (inlet) while O_2 was carrier gas (C_{O2} > 66 vol%, M_{catal} = 27.9 mg, T = 293 K), (B) as a function of O_2 while CO was carrier gas (C_{CO} > 87 vol%, M_{catal} = 19.3 mg, T = 293 K). Double logarithmic plots of both curves for determination of reaction rate and constant as insets (units retained).

Figure 4: (A) Temperature dependency of conversion of CO (2 vol% CO in O_2, M_{catal} = 27.9mg) (B) Arrhenius plot: natural logarithm of conversion versus the inverse temperature. A linear fit with very good precision reveals an apparent activation energy of 7.7 kJ/mol.

Figure 5: Calculated profile of CO concentration through the cross section of a npAu disk (0: outer surface, thickness 200 μm, $r_{capillary}$ = 15 nm) based on a reaction diffusion

model. The reaction dynamics/constant was based on the run of conversion for high oxygen partial pressures (Figure 3 (A)).

Figure 6: Titration of adsorbed atomic oxygen after treatment with ozone.

Figure 7: Left: Ag3d XP spectra. (A) after activation, (B) after exposure to 1 mbar CO for 1 hour, (C) after exposure to O_2 for 1 hour, (D) in-situ XPS at 1 mbar O_2, (E) in-situ XPS at 1 mbar CO/O_2 (1:1), (F) after the in-situ XPS measurements. The arrow marks the position of a transient signal component which appears only in the presence of the gas phase.

Right: Signal deconvolution of the in-situ XP spectra (D) and (E) from the left panel. The peaks under the signal component between 364 and 366 eV are displayed for illustrative purposes; they may not necessarily represent the full complexity of these signals.

Figures

Figure 1

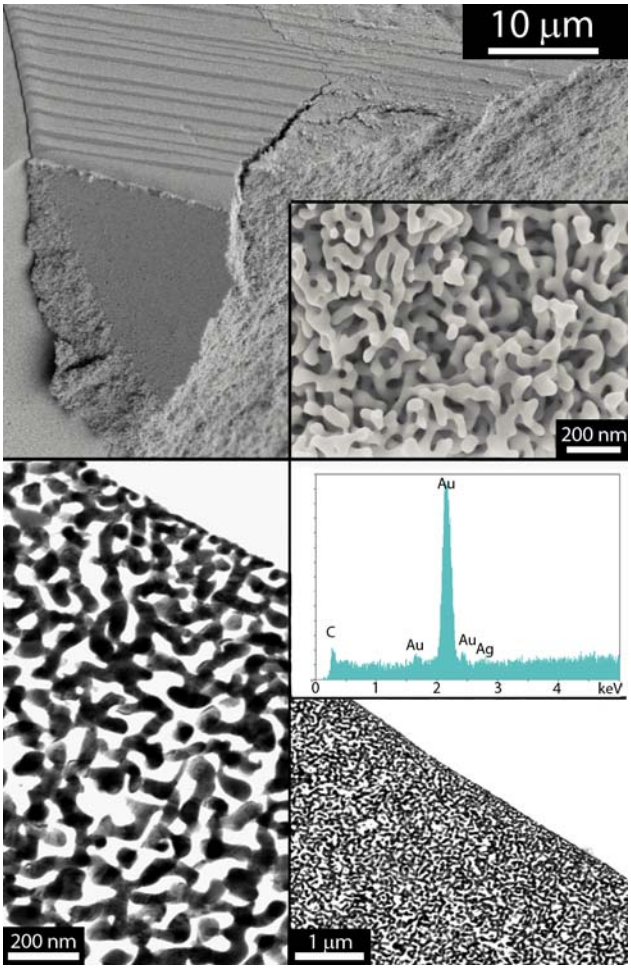

Figure 2

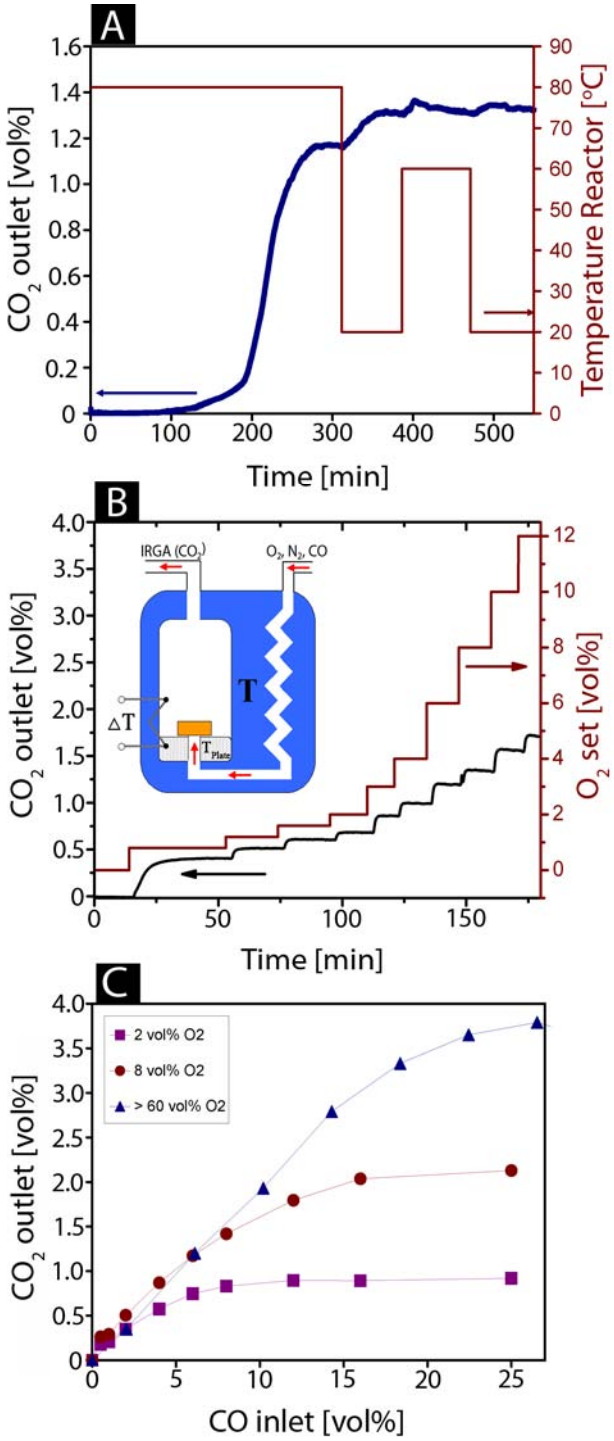
A
CO2 outlet [vol%]
Temperature Reactor [°C]
Time [min]
B
IRGA (CO2)
O2, N2, CO
T
ΔT
TPlate
CO2 outlet [vol%]
O2 set [vol%]
Time [min]
C
2 vol% O2
8 vol% O2
> 60 vol% O2
CO2 outlet [vol%]
CO inlet [vol%]

Figure 3

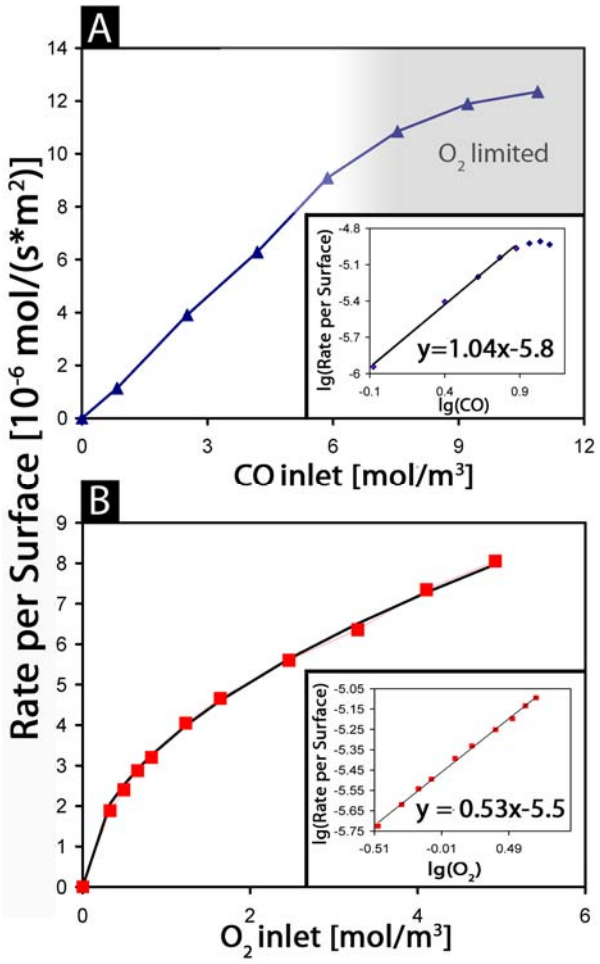

Figure 4

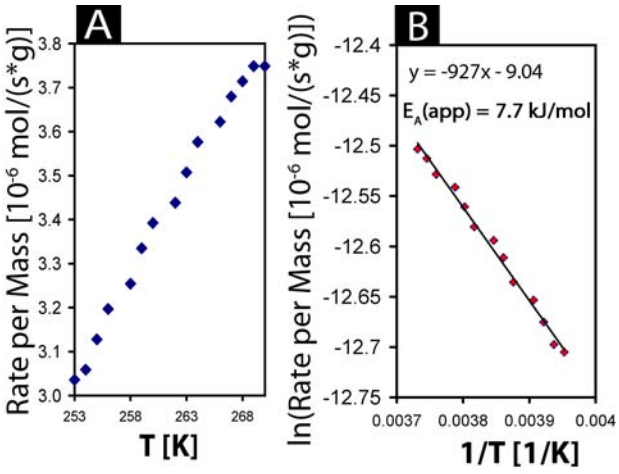

Figure 5

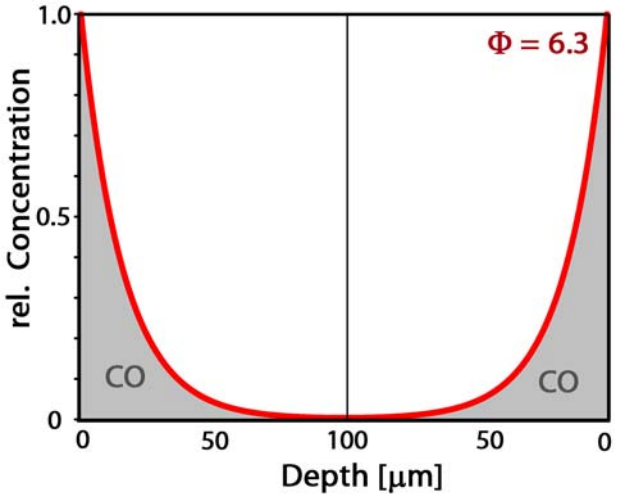

Figure 6

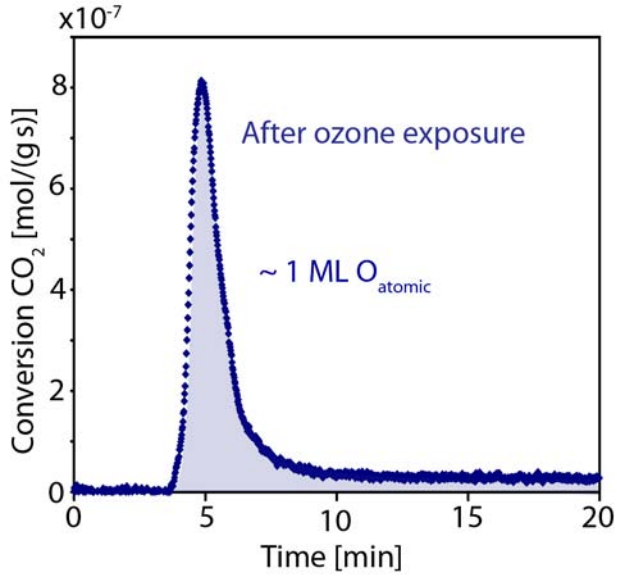

Figure 7

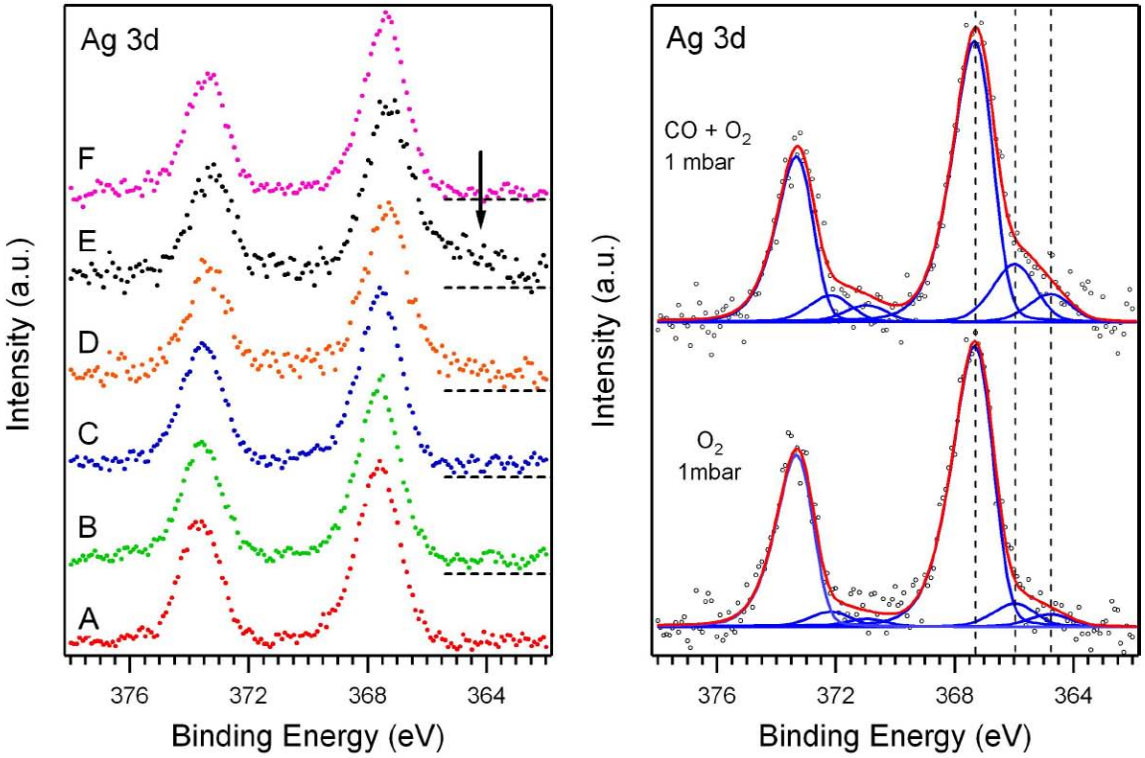
Ag 3d
F
E
D
C
B
A
Intensity (a.u.)
376
372
368
364
Binding Energy (eV)
Ag 3d
CO + O2
1 mbar
O2
1mbar
Intensity (a.u.)
376
372
368
364
Binding Energy (eV)